RESEARCH ARTICLE

Circumferential spicule growth by pericellular silica deposition in the hexactinellid sponge *Monorhaphis chuni*

Xiaohong Wang[1,2], Matthias Wiens[1], Heinz C. Schröder[1], Klaus P. Jochum[3], Ute Schloßmacher[1],
Hermann Götz[4], Heinz Duschner[4] and Werner E. G. Müller[1,*]

[1]ERC Advanced Grant Research Group at the Institute for Physiological Chemistry, University Medical Center of the Johannes
Gutenberg University Mainz, Duesbergweg 6, D-55128 Mainz, Germany, [2]National Research Center for Geoanalysis,
26 Baiwanzhuang Dajie, Beijing CHN-100037, China, [3]Max-Planck Institute for Chemistry, Postbox 3060, D-55020 Mainz,
Germany and [4]Institute of Applied Structure- and Microanalysis, University Medical Center of the Johannes Gutenberg-University,
Obere Zahlbacherstr. 63, Geb 911, D-55131 Mainz, Germany

*Author for correspondence (wmueller@uni-mainz.de)

SUMMARY

The giant basal spicule of the hexactinellid sponge *Monorhaphis chuni* represents the longest natural siliceous structure on Earth. This spicule is composed of concentrically arranged lamellae that are approximately 10 μm thick. In the present study, we investigated the formation of outer lamellae on a cellular level using microscopic and spectroscopic techniques. It is shown that the formation of an outermost lamella begins with the association of cell clusters with the surface of the thickening and/or growing spicule. The cells release silica for controlled formation of a lamella. The pericellular (silica) material fuses to a delimited and textured layer of silica with depressions approximately 20–30 μm in diameter. The newly formed layer initially displays 40 μm wide, well-structured banded ribbons and only attains its plain surface in a final step. The chemical composition in the depressions was studied using energy dispersive X-ray spectroscopy and by staining with Texas Red. The data suggest that those depressions are the nests for the silica-forming cells and that silica formation starts with a direct association of silica-forming cells with the outer surface of the spicule, where they remain and initiate the development of the next lamellae.

Key words: spicule, *Monorhaphis chuni*, Hexactinellida, sponge, pericellular silica formation.

INTRODUCTION

Silicate- and/or silica-depositing organisms are found throughout the prokaryotic and eukaryotic world (reviewed in Müller, 2003; Ehrlich, 2010; Ehrlich et al., 2010a). Whereas prokaryotic organisms require a supersaturated silica environment to induce precipitation of amorphous silica during the exponential growth phase (Inagaki et al., 2003), eukaryotic organisms are able to accumulate silicate to concentrations that allow its polycondensation within their cell(s). Plants have the capacity to take up silicic acid in the range of 0.1 to 0.6 mmol l^{-1} from the soil in their rhizosphere; they then translocate this monomeric ortho-silicic acid to their branches and deposit it as amorphous silica or poly(silicate), also termed biosilica (Morse, 1999; Müller et al., 2008e), in their cell walls (Ma, 2003) or in cell vacuoles (Neumann, 2003). Diatoms (unicellular algae) accumulate silicic acid from the aqueous milieu *via* specific transporters at concentrations of up to 340 mmol l^{-1} (Hildebrand and Wetherbee, 2003) and deposit it in special vesicles from where it is channeled onto distinct proteins (Perry, 2003), e.g. silaffins (Kröger and Sumper, 2000), and also onto chitin (Brunner et al., 2009).

Among the metazoans, the siliceous sponges (Porifera: Demospongiae and Hexactinellida) are the only taxa that build their skeleton (spiculae) of amorphous silica (Morse, 1999; Uriz, 2006; Müller et al., 2007d; Ehrlich et al., 2010b). Their silicification deposition–polycondensation pathway is distinguished from others by their ability to take up and accumulate silicic acid from a very silicon-poor aqueous environment (5 μmol l^{-1}) (Maldonado et al.,

2005) *via* a special transporter (Schröder et al., 2004) in vacuoles (silicasomes) (Schröder et al., 2007), and to subsequently polycondensate silicic acid enzymatically to biosilica (Morse, 1999) or poly(silicate) (Müller et al., 2008e). A further characteristic of sponge spicule formation is that only a few genes control the formation of this inorganic matrix, poly(silicate). The major genes involved are the silicateins, a family of genes that encode the poly(silicate)-forming enzyme (Shimizu et al., 1998; Cha et al., 1999; Krasko et al., 2000; Müller et al., 2007b), and the silintaphins. In the center of the spicules within axial canals, axial filaments exist both in Hexactinellida (Müller et al., 2008c) and in Demospongiae (Shimizu et al., 1998); the main component of the axial filaments is the silicateins. In addition, silintaphin-1 has been identified, which functions as a silicatein interactor and stabilizes silica nanoparticles under formation of silica nano- and micro-fibers and/or rods (Wiens et al., 2009). Furthermore, silintaphin-2 likewise interacts with silicatein and might serve as a final member of a signal transduction chain that controls spiculogenesis (Wiens et al., 2011). Post-transcriptional modifications of silicateins, primarily *via* phosphorylation, likely also affect the shape, size and form of axial filaments (Müller et al., 2005; Müller et al., 2007a).

The spicules of sponges display an amazing diversity of forms (Boury-Esnault and Rützler, 1997; Uriz et al., 2003; Uriz, 2006; Ehrlich, 2011). This remarkable and striking polymorphism of spicules, which is genetically controlled, is used in taxonomy as one of the major species characteristics of sponges (Hooper, 1997).

The formation of siliceous spicules starts intracellularly in vesicles with the formation of an axial filament composed of silicatein, around which the first layer of poly(silicate) is deposited (Mugnaioli et al., 2009; Müller et al., 2005). The resulting immature rods are extruded from the spicule-forming cells (sclerocytes) into the extracellular space, the mesohyl, where they grow in length and width. The longitudinal growth of the spicules is promoted by elongation of the axial filament through the addition of silicatein molecule units, which exist in the mesohyl, to the tip(s) of the spicules. In hexactinellids, the axial canal of (most) spicules remains open at the tips (Schulze, 1904; Müller et al., 2007c), whereas in demosponges the axial canal of the mature spicules is usually sealed by silica (Minchin, 1909). However, even some demosponge species possess mature spicules with open axial canals, e.g. the dichotriaenes of *Erylus mammillaris* (W.E.G.M., personal observation). The lateral growth of the spicules, i.e. the thickening, proceeds in demosponges (Schröder et al., 2006) and hexactinellids (Wang et al., 2007; Müller et al., 2007e; Müller et al., 2009b) by appositional layering of silica cylinders, guided by galectin and collagen. The required building elements for poly(silicate) formation in the lateral direction (lamellae formation) are the initially intracellularly located silicatein(s) and the substrate monomeric/oligomeric silicate released from the cells (Müller et al., 2005; Schröder et al., 2006; Schröder et al., 2007). It has been postulated that during appositional growth the silicate substrate is released from the sclerocytes and used by silicatein to form the poly(silicate) lamellae (Schröder et al., 2007).

It should be mentioned that biosilica polycondensation in vitro is driven enzymatically (Cha et al., 1999; Krasko et al., 2000; Müller et al., 2008c) under physiological natural concentrations of silica ($<1\,\mathrm{mmol\,l^{-1}}$; pH ~7) whereas higher concentrations ($\geq 4.5\,\mathrm{mmol\,l^{-1}}$ Na-silicate) are needed for polycondensation in the absence of the enzyme (Ehrlich et al., 2008; Ehrlich et al., 2010c). However, until now, no detailed experimental data or observations describing the morphogenetic events controlling the appositional layering of the silica cylinders along the axial biosilica rod have been presented. Likewise unknown are the processes that allow the formation of spines and tubercles existing on the central rods of the spicules, and characteristic rays originating from them, like in the spicules classed according to major architectural types, e.g. the monaxons, tetraxons or triaxons (Butler, 1961). Some progress has been made recently to describe the bio-sintering process, e.g. fusion of distinct biosilica layers within spicules from demosponges and fusion of different spicules in hexactinellids to form combined interlocked frameworks (Müller et al., 2008d; Müller et al., 2009a).

It is difficult to elucidate the processes culminating in the characteristic morphology of the extracellularly located spicules in demosponges because spicule formation is a rapid process. In the demosponge *Ephydatia fluviatilis*, the spicules grow at a speed of $5\,\mu\mathrm{m\,h^{-1}}$ (Weissenfels, 1989). The short annual growth phase during which the spicules are formed makes studies of the concerted actions of the spicule-forming cells even more difficult. One technique that has been used in the past is following the development of the spicules in the three-dimensional cell culture system (primmorphs) (Müller et al., 2005). Using this approach, researchers inferred that the appositional growth involves an organic cylinder composed of galectin, into which biosilica is extruded (Schröder et al., 2006). However, it was not yet possible to study the major structural and functional components governing the coordinated movement and assembly of the sclerocytes, or the synthesis of the spicules in time and space. Only through the use of the giant basal spicule (GBS) from the hexactinellid giant sponge *Monorhaphis chuni* was a partial description of the molecular, cellular and functional processes made possible (reviewed in Wang et al., 2009a). According to isotope ratio measurements, the specimens of this deep-sea sponge species can reach ages far older than 1000 years (K.P.J., unpublished data), during which they form those giant spicules that can reach 3 m in length and 12 mm in diameter (Levi et al., 1989; Wang et al., 2009a). *Monorhaphis chuni* specimens grow with their cylindrical, round- to oval-shaped body around the middle to upper part of the GBS and anchor with the basal, i.e. oldest, part of the GBS to the seafloor (Fig. 1A,E).

In the present study, we analyzed the surfaces of the lamellarly organized GBS in those regions that are in life covered by tissue using optical and electron microscopic techniques coupled with spectroscopic analyses. These regions are involved in thickening of the spicules (Wang et al., 2009a). Our analyses show for the first time the involvement of the sclerocytes in the genesis of the biosilica lamellae; previously it was assumed that silicatein and its substrate were extruded into an organic cylinder surrounding the growing spicule (Schröder et al., 2006). In the present study, we did not investigate the other relatively large spicule type in *M. chuni*, the tauactins, as they are even more intimately surrounded by the sponge tissue than the GBS (Müller et al., 2007a), a fact that could evoke artifacts. A detailed description of the GBS, depicted in Fig. 1, is given in the Discussion.

The data presented here indicate that small clusters of sclerocytes exist on the surfaces of the spicules and promote the deposition of poly(silicate) onto the existing lamella. After completion of one lamella, the cells remain on the surface and are then possibly available for a further round of lamella formation. We term the complete process of lamellar construction in the GBS 'circumferential pericellular spicule formation'. The fact that silicatein deposits biosilica on cell surfaces has been demonstrated previously in *Escherichia coli* that were transfected with silicatein (Müller et al., 2008a). In silicate-containing culture medium, those genetically modified bacteria were shown to synthesize a biosilica coat.

MATERIALS AND METHODS
Sponge and GBSs
Specimens of the hexactinellid *Monorhaphis chuni* Schulze 1904 (Porifera: Hexactinellida: Amphidiscosida: Monorhaphididae), the species that forms the GBSs, were collected in the South Chinese Sea from a depth of 1110 m; the longest GBS found in 2008 measured 2.7 m in length and 12 mm in diameter (Fig. 2A). The spicules had been sealed in plastic bags and were stored at 4°C (cold room in the Institute of Oceanology, Chinese Academy of Sciences, Qingdao, China) since the date of collection. The spicules had not been freed from the (partial) organic coat by mechanical cleaning or detergents (sodium dodecyl sulphate) (Müller et al., 2007c; Wang et al., 2008). Among those spicules, one sample that measured 2.5 m in length and 7 mm (maximum) in diameter was selected for the analyses summarized here.

Digital light microscopy
The analyses were performed with a VHX-600 Digital Microscope from KEYENCE (Neu-Isenburg, Germany), equipped either with a VH-Z25 zoom lens (25× to 175× magnification) or a VH-Z-100 long-distance high-performance zoom lens (up to 1000× magnification) (Wang et al., 2009b).

Microtomography analysis
The microtomography (μ-CT) analyses were performed as described previously (Wang et al., 2008) using a Desktop Cone-Beam μ-CT Scanner (lCT40, SCANCO Medical AG, Brüttisellen, Switzerland).
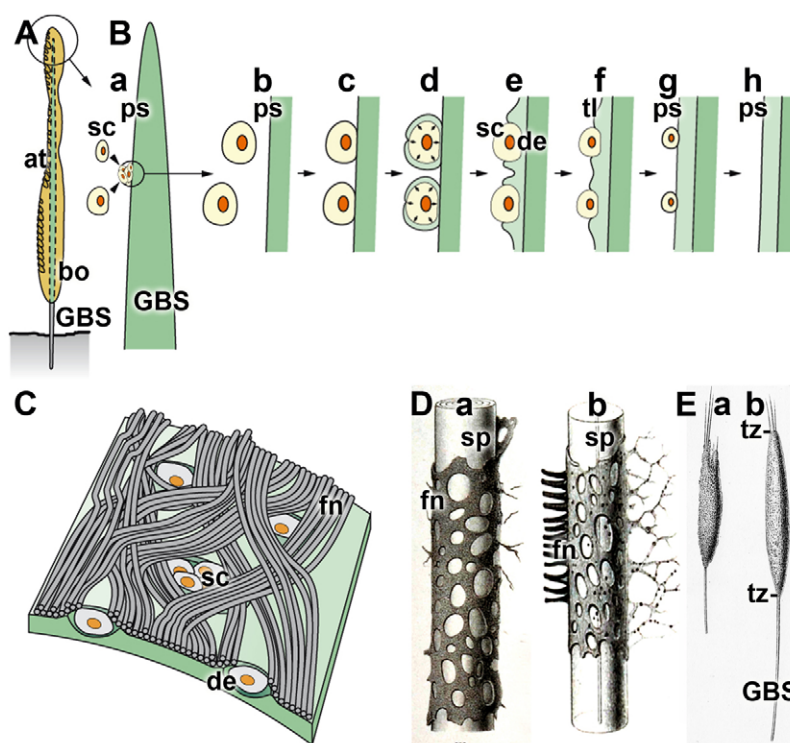
Fig. 1. Schematic representation of a giant basal spicule (GBS), formed by *Monorhaphis chuni*, and its pericellular circumferential growth pattern. (A) The cylindrical/oval body (bo) of *M. chuni*, interspersed with many atrial openings (at), surrounds the GBS. (B) Pericellular circumferential lamella formation. (B-a–B-c) It is proposed that, during appositional growth of the GBS, sclerocytes (sc) cluster together and attach to the surface of the existing lamellae with a smooth/plain surface (ps). The sclerocytes start to extrude silicic acid that is converted extracellularly by silicatein to a poly(silicate) coating (B-d). With the progression of the pericellular silicification, a new outer lamella with depressions (de) is formed. Those depressions are explained as imprints caused by the poly(silicate)-forming sclerocytes (B-e). Subsequently, the existing depressions fuse (B-f) under formation of a textured lamella (tl). (B-f) The circumferential pericellular lamella formation is terminated after completion of a plain surface. (B-g) In the later stage, the sclerocytes detach from the completed plain surface (B-h). (C) 'Immobilization' of the clusters of sclerocytes by a fibrous network (fn) embedded in depressions. (D-a,D-b) The coating of the GBS and the related spicules (sp) in *M. chuni*, the comitalia, with a fibrous network (fn) have already been sketched by Schulze (Schulze, 1904). The formation shown in D-a is a more progressed stage of lamella formation than that shown in D-b. (E) The same author (Schulze 1904) already described that young specimens of *M. chuni* grow around one GBS. (E-a) This drawing represents a younger specimen than that shown in E-b. At the top of the specimens, spicules, including the GBS, protrude from the body of the specimens that are not covered by tissue. The transition zones (tz) between the body and the naked spicules are marked; there the formation of the lamellae starts.

EDX spectroscopy

Energy dispersive X-ray spectroscopy (EDX) was performed with an EDAX Genesis EDX System attached to a scanning electron microscope (Nova 600 Nanolab; FEI, Eindhoven, The Netherlands) operating at 10 kV with a collection time of 30 s. Areas of approximately $20 \mu m^2$ were analyzed by EDX as described by Wang et al. (Wang and Müller, 2009; Wang et al., 2009b) and by Wiens et al. (Wiens et al., 2010).

Labeling procedure with Texas Red

Texas Red sulfonyl chloride (Molecular Probes, Eugene, OR, USA) was used for conjugation with macromolecules present on the surface of the GBS. The conjugation procedure was performed at pH 9.0 as described previously (Titus et al., 1982; Panchuk-Voloshina et al., 1999). After washing with PBS, the samples were inspected with a KEYENCE BZ-8000 Epi-fluorescence Microscope using an S-Plan-Fluor 20× lens. The filter setting 'ex 560±40–em 630±60 nm' was used to detect the signals. In a control series, the spicules were pre-treated with $20 \mu g ml^{-1}$ Proteinase K (Sigma-Aldrich, Taufkirchen, Germany) at 37°C for 2 h in $10 mmol l^{-1}$ Tris-HCl buffer (pH 8.0; $100 mmol l^{-1}$ ethylenediaminetetraacetic acid, $50 mmol l^{-1}$ NaCl, 0.5% sodium dodecyl sulphate). Experimental samples, which were not treated with Proteinase K, were incubated with the same buffer and under the same incubation conditions and were subsequently coupled to Texas Red (Sigma-Aldrich).

Determination of the hardness of the silica layers

Micro-hardness determination of the silica layers was performed by application of the nanoindentation method with a NanoTest 550 indentation system (Micro Materials Ltd, Wrexham, UK) as described previously (Li and Bhushan, 2002). This equipment was connected to a sharp Berkovich diamond indenter with a tip radius of 200 nm. Prior to analysis, the spicule was sliced into ~3 mm thick sections that were subsequently polished (Müller et al., 2007c). The spicule of *M. chuni* used for this analysis had a diameter of 7 mm. Sample slices were embedded in epoxy resin. Finally, the determination of the hardness was performed applying a surface approach velocity of $5 nm s^{-1}$; the depth limit was 1500 nm.

LA-ICP-MS analysis

Laser ablation inductively coupled plasma mass spectrometry (LA-ICP-MS) analysis was performed with a sector-field ThermoFinnigan Element 2 mass spectrometer equipped with a New Wave UP 213 laser ablation system (Max Planck Institute for
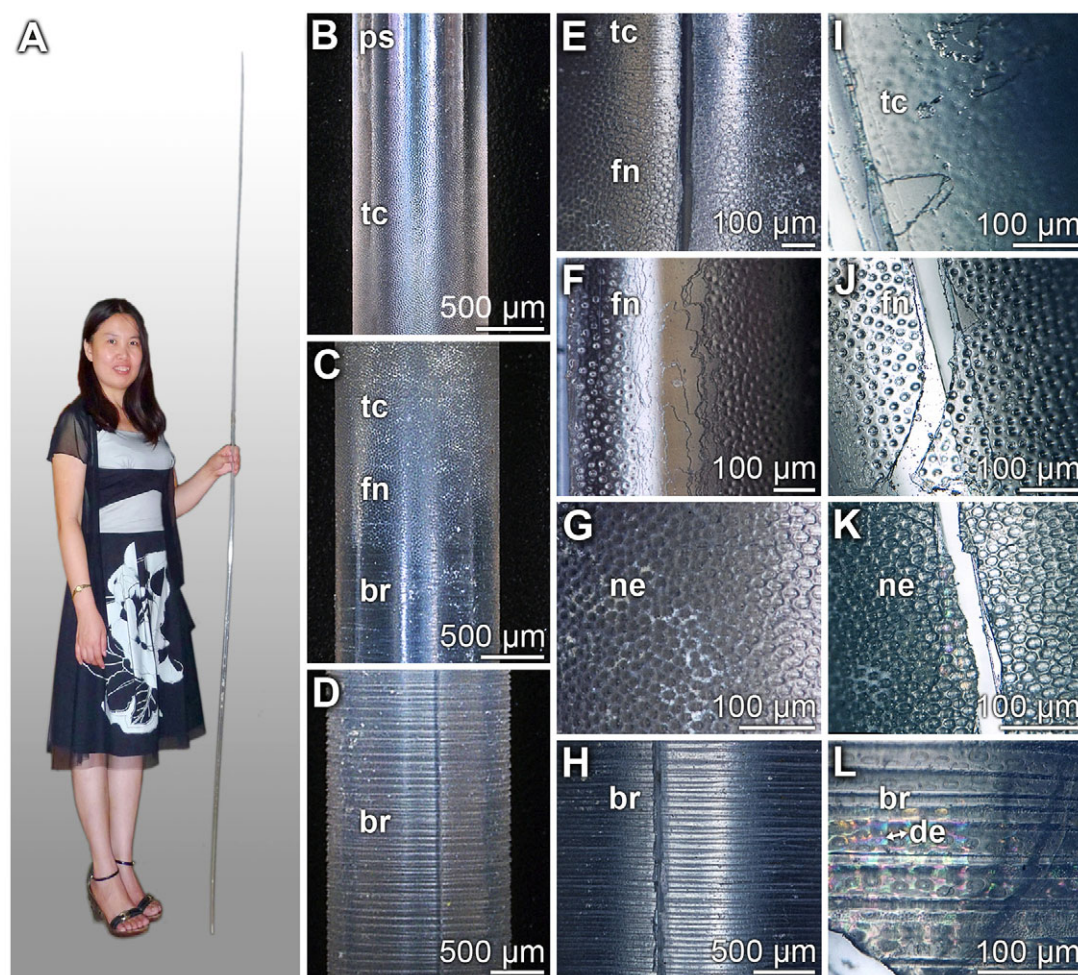
Fig. 2. Surface silicification pattern of giant basal spicules (GBS) from *Monorhaphis chuni*. (A) GBS 2.7 m in length and 12 mm in diameter. (B–D) Distinct order of structures seen on the surface lamella of the spicule. The tip of the spicule shows a smooth/plain surface (ps), followed by a zone of tiny coarse protrusions (tc), a thin layer of a finely woven network (fn), and finally a zone characterized by banded ribbons (br) that entwist the spicule. (E,F,I,J) Higher magnification of the transition from the tiny coarse structures to the finely woven network, showing depressions. (G,K) The network (ne) shows distinct walls around the cavities. (H,L) After 5 cm from the beginning of the structured silicification layer the surface turned to banded ribbons. (L) One depression is marked with a double arrow. (B–L) Digital light microscopic images.

Chemistry, Mainz, Germany) (Müller et al., 2008b). Spot sizes of 50 μm were selected on sections of the GBS. The internal standard element was Si, as described previously (Müller et al., 2008b). Calibration was performed with NIST SRM 612 glass (Standard Reference Materials Program NIST, Gaithersburg, MD, USA), using the values published in the GeoReM database (http://georem.mpch-mainz.gwdg.de). The detection limits ranged between 0.3 and $10 \, \text{ng} \, \text{g}^{-1}$. Five parallel series of experiments were performed; the mean values (±s.d.) and the respective statistical significances were determined as described previously (Sachs, 1984).

RESULTS
GBSs and their surface silicification pattern
By inspecting the surface of the GBS at the transition between the tissue-free and tissue-covered zones, a gradual emergence of variously structured and porous areas was seen (Fig. 1D, Fig. 2B–D). The tissue-free zone of the GBS (2.5 m long and a maximum of 7 mm wide) used here, measured 8.5 cm from the tip, and a smooth surface was observed (Fig. 2B). From this zone towards the part of the GBS that in life was tissue-covered, structured areas appeared that comprised distinct sequences of structural patterns. The surface showed fine, reflecting irregularities (Fig. 2B) that resolved, at high light microscopic magnification, as a continuous thin layer riddled with depressions with elevated rims (Fig. 2E,I). In continuation of this zone, the surface of the spicule appeared as a finely woven network (Fig. 2F,J). The rims of the indentations develop into distinct

walls (Fig. 2G,K). The diameters of the round fairly uniform depressions varied between 23 and 38 μm. The arrangement of the indentations was not regular (Fig. 2G,K). Finally, further away from the tip, the surface showed a transition to a zone of banded ribbons that almost perfectly encompassed the spicule (Fig. 2H,L). The widths of the ribbons varied between 31 and 56 μm. It should be stressed that ribbons that were closer to the network were translucent and the depressions shone through (Fig. 2L).

Surface silicifying layering
μ-CT analysis was employed to identify the patterns on the silicifying surface layers (Fig. 3A). A reconstruction revealed that those silicifying surface layers bind tightly to the subjacent, penultimate lamella of the spicule. During growth of a new surface layer of the GBS, the surface of the penultimate lamella is cluttered with tiny bumps. Such layers are found in the transition zone between the plain spicule surface and a newly forming lamella, close to the border of the sponge body tissue and the naked spicule (Fig. 1E). At a later stage the penultimate lamella becomes perfectly smooth and the surface lamella can easily mechanically be detached from it (Fig. 3B). Often the more centrally located lamellae (Fig. 3D), in addition to the surface lamella and the penultimate lamella (Fig. 3C), are visible at fracture sites. As shown in Fig. 3C, the surfaces of the lamellae change from more textured (at the surface lamella) to smooth in the more centrally located lamellae. The plain lamellae and the axial cylinder are covered by the tiny coarse layer, which
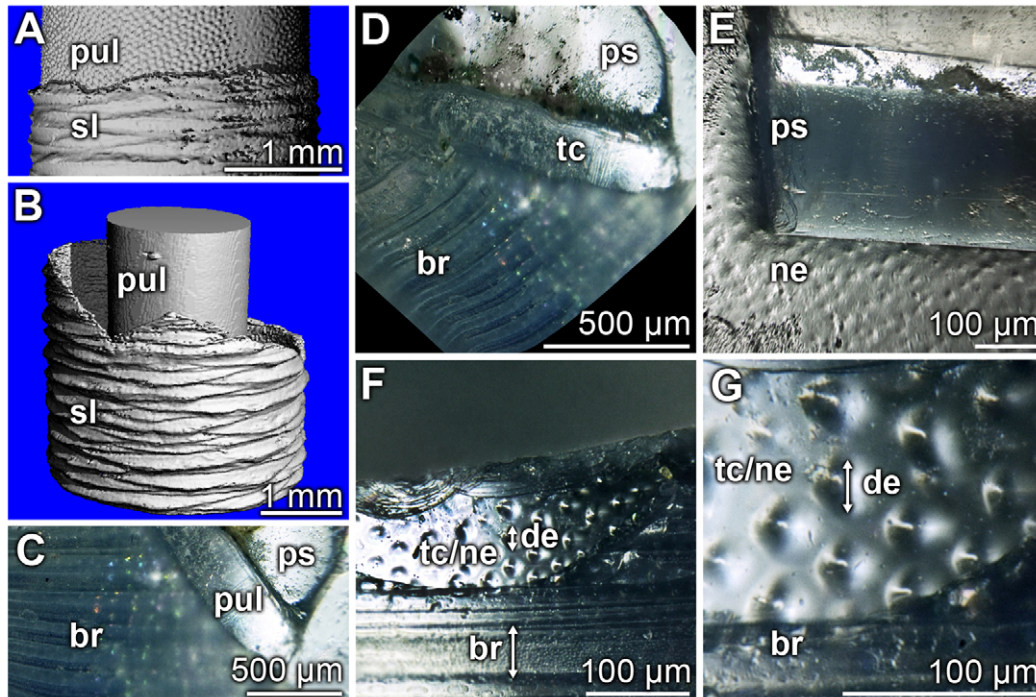
Fig. 3. Distinct construction of the surface silicificating layer visualized by (A,B) µ-CT analysis or (C–G) optical microscopy. (A) The µ-CT reconstruction of a region comprising a growing surface layer (sl) localized closer to the transition zone from the plain spicule surface to newly forming lamella. The surface of the penultimate lamella (pul) has a knobbed surface. (B) Further down the GBS, the surface lamella is less tightly attached to the penultimate lamella, very likely because of its plain surface. (C,D) Frequently, the penultimate lamella, here with tiny coarse structures (tc), and the lamellae underneath, here with the smooth/plain surface (ps), can be distinguished. The surface is formed by the banded ribbons layer (br). (D) The same region as that shown in C shown in a tilted view. (E–G) Often a lamella with the plain surface is surrounded by a tiny coarse layer that is combined with the network (ne). The width of one ribbon and the diameter of one depression are marked (double-headed arrow; de).

also includes the fine network around which the banded ribbons are circulating (Fig. 3E,F). At a higher magnification (Fig. 3F), the network around the plain rod and the banded ribbons are illustrated in a tilted view. This image also shows that the widths of the ribbons, 31 to 56 µm, are slightly larger than the diameters of the depressions (23–38 µm).

Element distribution resolved by EDX spectroscopy in the surface layer

In order to identify the chemical composition of the lamellar surface region, scanning electron microscopy (SEM) images were taken at different depths from the surface and, in parallel, the corresponding EDX spectra were recorded (Fig. 4). For this analysis, the spicule sample was moderately bent to induce cracking of the outer layers, as described by Müller et al. (Müller et al., 2008d) (Fig. 4A,B). The SEM images were obtained from different depths below the surface. All corresponding EDX analyses that were taken from more centrally located lamellae, approximately 30 layers from the surface (Fig. 4C-a), approximately 20 layers from the surface (Fig. 4D-a), or from the penultimate lamella (Fig. 4E-a) gave almost identical EDX spectra with dominant peaks for Si and O, reflecting the biosilica matrix (Fig. 4C-b–E-b). Only the EDX spectrum (Fig. 4F-b) obtained from the surface of the banded ribbon layer (Fig. 4F-a) gave a more diverse distribution. Besides Si and O, indicating the presence of silica (SiO_2), surface layers are composed of traces of organic material, as assessed from the presence of the peaks for Na, Mg, S, Cl, K and especially C. We have previously

described the banded ribbon structure as an organic layer (Wang et al., 2008).

Element analysis of the depressions within the ribbons

The spicule surfaces in the central part of the sponge body display a pronounced banded ribbon-like structure (Fig. 5A). It is striking that the ribbons have two appearances: non-perforated and perforated. Approximately 10 non-perforated ribbons are followed by approximately 20 perforated ribbons (Fig. 5A,B). The widths of the ribbons (31–56 µm) are slightly larger than the diameters of the depressions (23–38 µm; Fig. 5C,D). Optical microscopic analyses showed that the depressions are filled with ball-like structures (~10 µm). However, when these depressions were inspected by SEM (Fig. 5F), no structures within the holes could be resolved. This finding suggests that the ball-like structures were destroyed by the electron beam used for SEM analysis (10 kV). In order to obtain insight into the chemical difference between the smooth/plain regions within the ribbons and their depressions (Fig. 5E-a), EDX analyses were performed in parallel. The EDX spectra revealed that the smooth/plain regions only gave peaks for Si and O (Fig. 5E-b), reflecting silica, whereas the depression regions comprised dominantly peaks for elements characteristic for organic matter, e.g. C, Na, Mg, S, Cl and K (Fig. 5F-b). Two other biogenic elements, P and N, are not marked in Fig. 5F-b, as their signals cannot be unequivocally assigned. It is very likely that the N signal is shielded by the large C signal, whereas the (probable) P signal, at 2.0 keV, is very small. We hypothesize that those depressions might be filled with cells, or fragments of them.
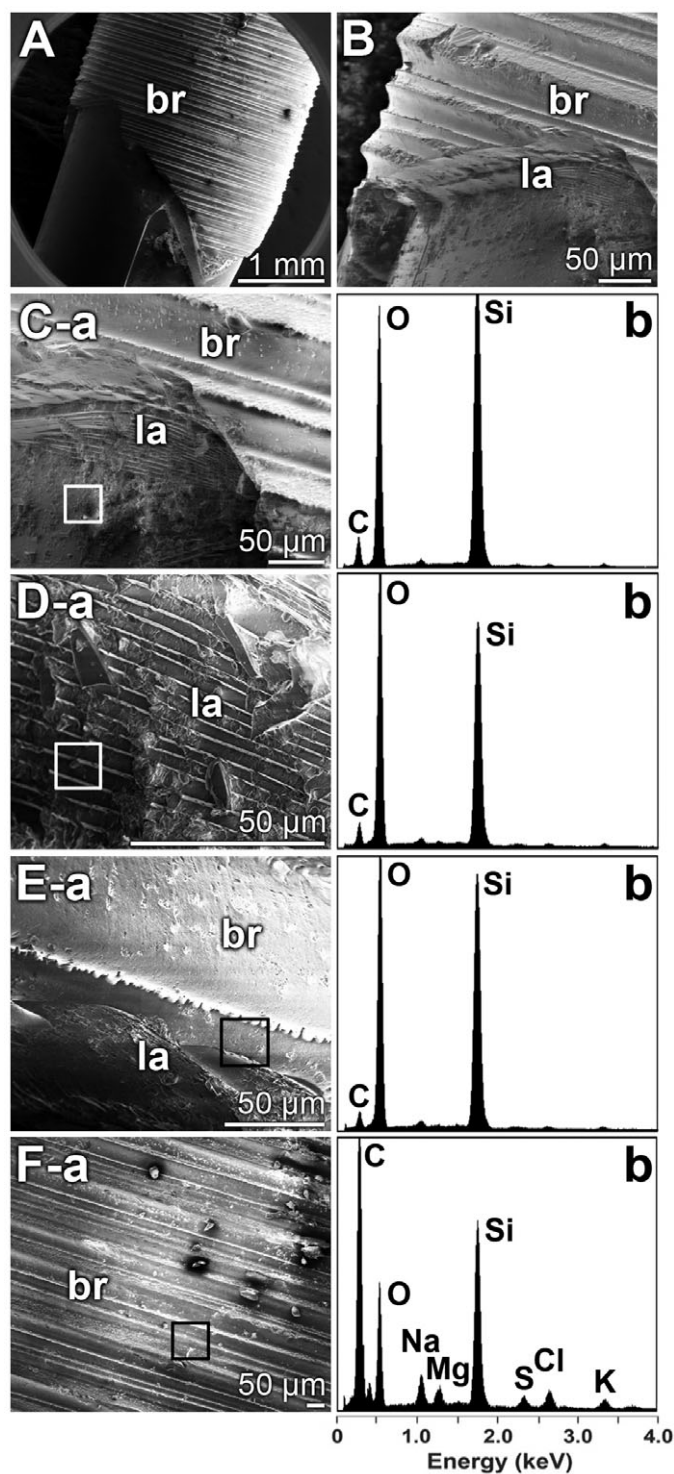
Fig. 4. Element analyses of different sites within the surface lamellar region. (A,B) Cross fracture through the spicule displaying the banded ribbon layer (br) and the sub-surface lamellar (la) architecture. SEM analyses. (B) Higher magnification of the image shown in A. (C–F) In parallel series, SEM images were taken from different sites of the surface (series a) and corresponding EDX analyses were performed to determine the element composition (series b). (C) Determination at the sub-surface region, approximately 30 layers from the surface. (D) SEM/EDX analysis in the lamellar zone, approximately 20 layers from the surface. (E) Surface, penultimate lamella region and (F) SEM/EDX analysis from the surface of the banded ribbons (br) zone. The areas that were selected for EDX analysis are marked (square) in the corresponding SEM image.
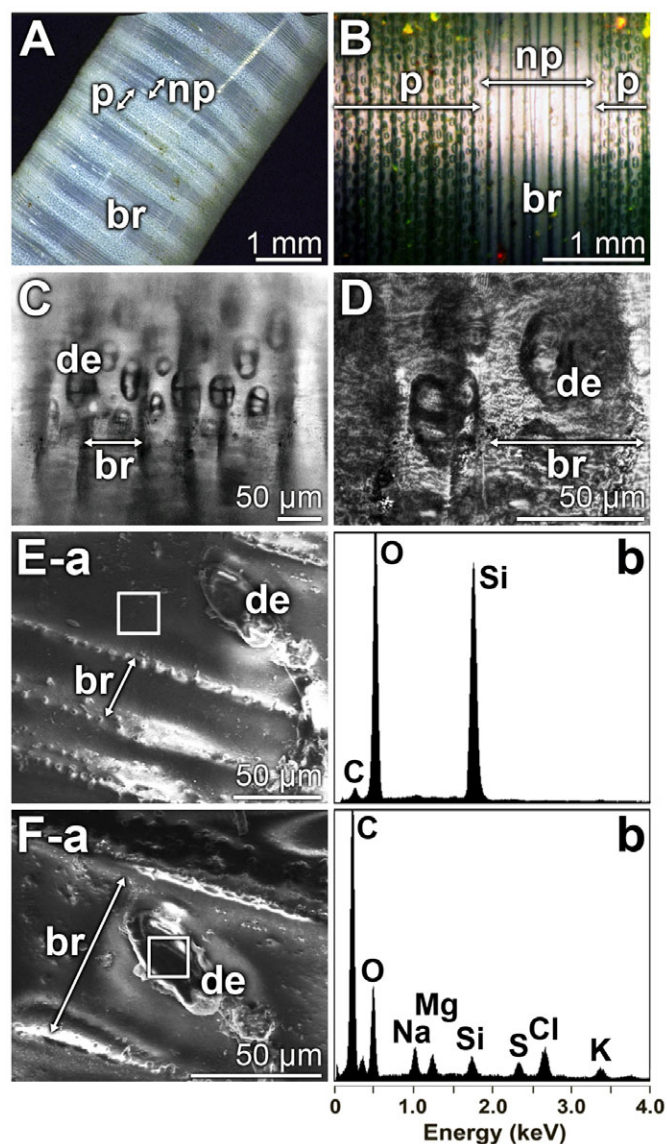

Fig. 5. Element analyses within the banded ribbon (br) layers. The surfaces of the samples were inspected by optical microscopy (A,B) to demonstrate the ordered sequence of ribbon structures (br) of non-perforated ribbons (np) [not provided with visible depression] and perforated ribbons (p) [with depressions (de)]. (C,D) At higher magnification, ball-like structures were visible within the depressions. The widths of the ribbons are marked with double-headed arrows. EDX analysis of the plain surface of a banded ribbon (E) and the depression existing within the band (F). Parallel studies by SEM inspection (series a) and EDX spectroscopy (series b) were performed.

Staining the content matter in the depressions for organic matter

In an attempt to verify that organic matter potentially exists in the depressions, the spicules were stained with Texas Red. As shown in Fig. 6A,C, bright signals were seen within the depressions. In order to check whether the dye is indeed conjugated with a proteinaceous material, the spicule samples were pre-incubated with proteinase K. After that treatment, no significant signals could be detected (Fig. 6B,D).
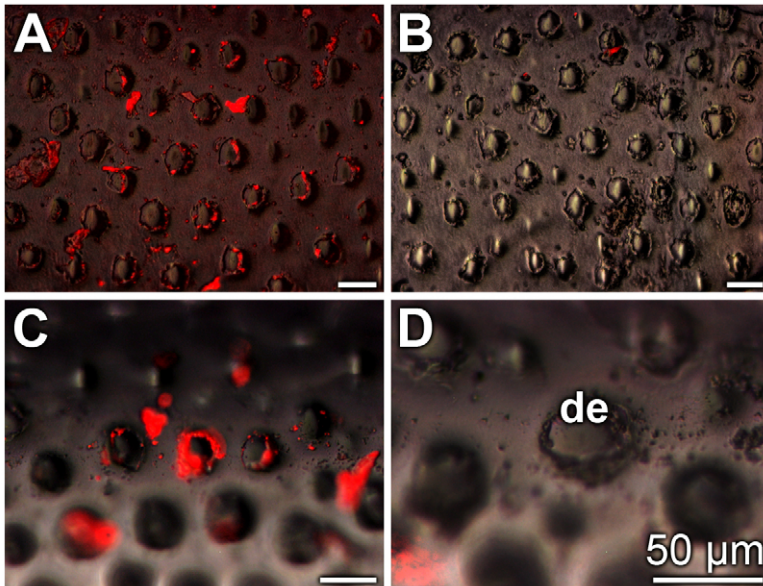
Hardness measurements

Hardness measurements were performed on the surfaces of polished slices from a GBS. Two locations were selected: a spot within the surface layers (the lamellar region located within the first 20μm of the surface lamella towards the center) and a location within the lamellar region, as illustrated in Fig. 7A-a. The results of the two series of hardness measurements gave different distribution curves. The hardness in the surface/rim region had initially considerably lower values. A displacement into the surface of 300nm was caused even at ~1GPa; only at pressure values of 3.2GPa were the maximal displacement values reached. In contrast, the hardness of the more centrally located lamellar region had only a small increment from 2.5 to 3.3GPa before reaching maximum displacement values (Fig. 7A-b).

Element analysis

LA-ICP-MS was applied to determine the trace element distribution within the different segments [samples covered with banded ribbons (Fig. 7B-a) and those comprising plain surfaces (Fig. 7B-b)] of the GBS. The analyses were performed within 80μm spots from the surface regions, the lamellar region and the axial cylinder, as shown in Fig. 7A-a. The quantitative spectroscopic data revealed that, for the elements Ca and Mn (Fig. 7C-a) and also for Na and Mg (Fig. 7C-b), the concentrations were significantly higher in the surface layers of slices covered with banded ribbons than in samples taken from an uncovered area. No significant differences between the two samples of spicules were seen in the element concentrations determined in the lamellar or axial cylinder parts of the slices (Fig. 7C-a,b).

DISCUSSION

In the present study we used the GBS of *M. chuni* as a model to clarify whether the growth of the skeletal elements in the lateral direction is controlled by sclerocytes. By light microscopy analyses and subsequent SEM analyses it became evident that the surface lamellae of the GBS contain nests/rounded depressions that are filled with ball-like structures. Those structures reacted with Texas Red. A definite answer to whether the Texas-Red-positive staining (Suzuki et al., 1997) of the material within the depressions depicts intact mononuclear cells, syncytia or nuclear cell fragments cannot

be given at present. However, the existence of protein-containing material could be proven by digestion experiments using proteinase K. Operationally, we term the Texas-Red-positive material as 'cells'. The existence of organic material in the 23–38μm depressions has also been confirmed by EDX analysis. This series of measurements proved the existence of the elements C, Na/Mg and S in those regions. Based on the data it is assumed that those cells in the depressions form and continuously develop a rim of poly(silicate) around them. At the beginning of lamella formation, the arrangement of the rounded depressions containing the cells is not highly ordered. Using a biomimetic approach, we genetically modified bacteria with the *silicatein* gene and demonstrated that *E. coli* form a biosilica coat around their cell walls (Müller et al., 2008a). These findings imply that bacterial as well as sponge cells that express the *silicatein* gene have the capacity to synthesize biosilica on their surfaces. The mechanism by which silicatein, together with its silica substrate, is released from the cells remains to be determined. As both components (silicatein and silicic acid) are intracellularly compartmentalized in vesicles, we assume that they are co-exported onto the cell surfaces where polycondensation proceeds.

Within the course of lamella formation, the depressions become covered or surrounded by ribbons that are almost perfectly banded and exhibit highly uniform widths of approximately 40μm (31–56μm). At present we can only speculate about the mechanism by which the cells, with their surrounding silica envelope, are unified to form ribbon-like structures. Cells from most hexactinellids form a multinucleate syncytium during embryogenesis or later, during tissue formation, that ramifies throughout the sponge (see Leys et al., 2007). More specific, the spicule-forming sclerocytes have also been assumed to fuse to a 'sclerosyncytium' (Leys, 2003) as deduced from the observations of spiculogenesis in embryos from *Oopsacas minuta*. Because the cell-containing depressions are separated from each other, we have no reason to believe that all cells participating in lamella formation fuse to form syncytia. Nevertheless, secondary syncytia formation could explain the secondary organization of the cells to banded ribbons *via* syncytial trabecular strands. Unfortunately, until now, it has not been possible to perform cytological studies using *M. chuni* tissue because of the poor conservation of collected samples. Therefore, another line of
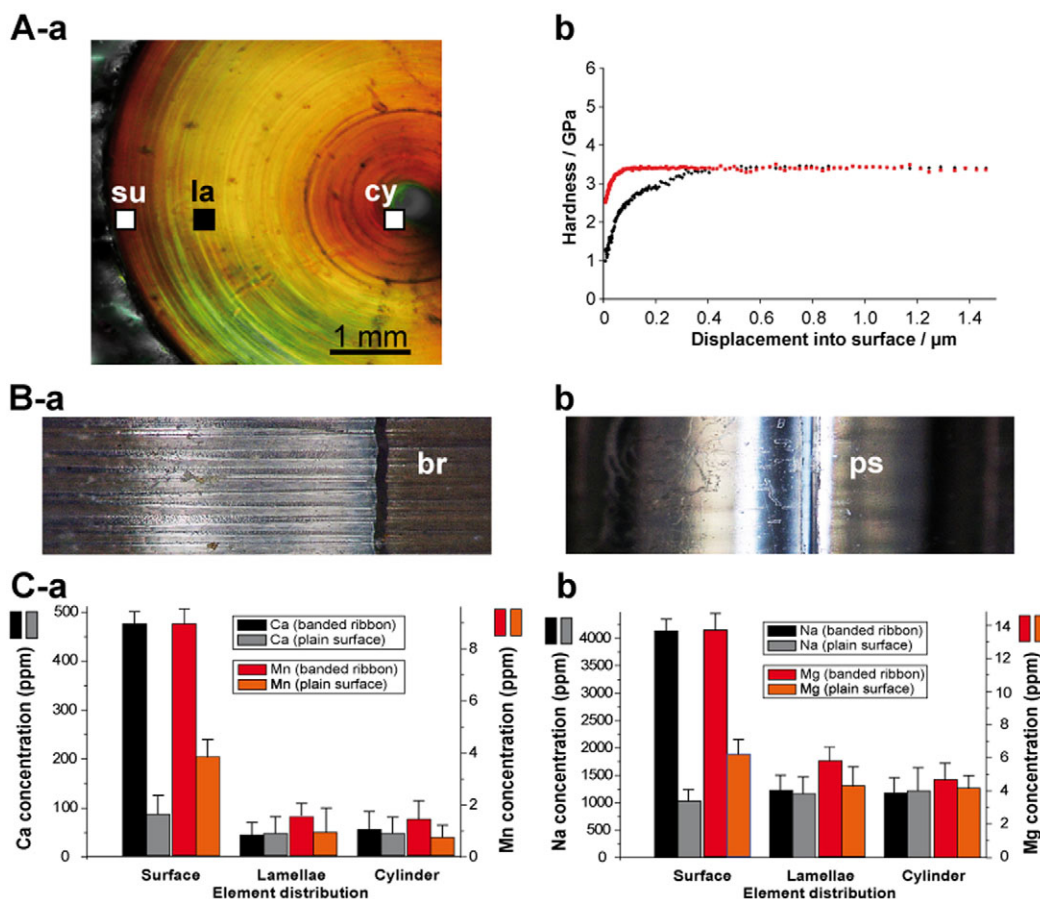
Fig. 7. Mechanical properties (A) and chemical composition (C) of the surface layers within the different regions of the GBS. (A-a) Cross-section through a GBS showing its three regions: the surface layers (su), the lamellar region (la) and the axial cylinder (cy). (A-b) Hardness values were determined as a function of displacement into the surface of a 7 mm thick GBS. The black curve gives the hardness values measured at the surface (20 μm from the rim) and the red curve those determined in the lamellar region, a more centrally located site. (B) Surface appearance of a spicule covered with banded ribbon structures (br) (a), and a view onto a smooth/plain surface (ps) of a spicule, not covered with a growing outer lamella (b). (C) Element analysis (LA-ICP-MS measurements) within sections, obtained from polished slices through spicules within the three morphological regions of the spicules (see panel A-a). The analyses were performed with spicules showing the banded ribbon structures and a region of a spicule that displays only a plain surface. The analyses were performed for Ca and Mn (C-a) and for Na and Mg (C-b). Please note the different scales for the respective elements.

explanation should be highlighted. Using the demosponge *Geodia cydonium*, it could be demonstrated that the extracellular mesohyl is rich in tubulin, which has the capacity to polymerize to microtubules (Reuter et al., 1987). Hence it may be hypothesized that the polymerization dynamics of microtubules could be the motor for the organization of the sclerocytes to ribbons.

Microscopic analyses suggest that the cell clusters in the depressions remain on the surface of the biosilica layer they formed. Initially they leave behind ~20–30 μm holes in the newly formed biosilica lamella, which had been visualized previously (Wang et al., 2008) (scheme shown in Fig. 1B-a–f). Those holes are closed after termination of the silicification process, resulting in the formation of perfectly concentric plain lamellae (Fig. 1B-g,h). No evidence could be found that suggests an embedding of the cells within the silica lamella. It appears to be more likely that the cells remain on the surface of the lamellae and can undergo further rounds of silica lamella formation. Such a mechanism is economic from the viewpoint of morphogenesis because during the progression of the thickening of the spicules, sclerocytes of the same differentiation state can be re-used. Moreover, the same signal regulatory network between those sclerocytes can be re-used; this aspect is crucial as

no elaborate cell junctions between sponge cells have yet been detected or elucidated (Müller et al., 2004). Following this line of argumentation, filamentous structures must exist to keep the sclerocyte clusters, after termination of silica deposition and after formation of a complete plain lamella, at their functional position. Recent studies (Wang et al., 2008; Ehrlich et al., 2008) have proposed, based on electron microscopic observations, that it is the collagen network that surrounds the outer surface of the spicules. That filamentous framework leaves open holes with diameters of 10 to 25 μm, matching exactly the diameters of the depressions in the banded ribbon layers. Previously, Schulze illustrated that *M. chuni* spicules are surrounded by filamentous sheaths comprising openings of unknown function (Schulze, 1904). It should be noted that for the first few centimeters from their tips, the spicules are not covered by silica lamellae containing cell fragments; this region is composed solely of smooth surfaces. This surprising observation was made by Schulze, who saw that even young *M. chuni* specimens showed spicules protruding from the body at the top end (Schulze, 1904) (Fig. 1E).

Our microscopic and spectroscopic/chemical analyses revealed that the surface silica layer(s) of the GBS from *M. chuni* differs

from the more internal layers by the existence of the cells located in the depressions that have been attributed to the formation of the lamellae. In order to examine whether the silicate matrix, formed at the surface of the spicules, also differs from the more centrally arranged lamellae in terms of inorganic chemical composition and mechanical properties, we applied the techniques of LA-ICP-MS spectroscopy and hardness/indentation determination. The spectroscopical analysis distinctly showed that the surface layers from spicule samples that were covered by banded ribbons comprised significantly higher concentrations of monovalent and divalent cations within the poly(silicate) than the silica that exists more centrally within the spicule. In the silica layers close to the surface, the silicic acid building blocks forming the silica layers exist, to a considerable extent, as salts of Na, Mg, Ca and Mn. Recently, we proposed that the silicatein-mediated synthesis of biosilica starts from the silicic acid/silicate substrate and proceeds *via* cyclic silicic acid species (trisiloxane rings) to poly(silicate) (Schröder et al., in press). As a consequence of the higher concentration of cations in the silica matrix of the outer surface of the spicules, the hardness should be lower (Wiederhorn, 1969; Müller et al., 2008b). This supposition was proven by hardness studies on cross-sections through the spicule. The data revealed that the near-surface lamellae from spicules surrounded by banded ribbons were more flexible (by a factor of two) compared with the lamellae that were not in the process of formation and were devoid of depressions. In turn, a mechanism has to be proposed that allows an understanding of the ageing process of poly(silicate) after formation of the surface-directed lamellae. The data of the present study show that with the progression of silica layering around the spicules of *M. chuni*, the cation content decreases. Hence it is assumed that, during ageing, the formation of siloxane (Si-O-Si) bonds through condensation (removal of water) of residual silanol (Si-OH) groups present in the biosilica lamellae will occur. As a consequence, cations that act as counter-ions to acidic silanol groups will be eliminated from the silica phase. The latter process could proceed in association with a cation exchanger, perhaps collagen carrying negatively charged residue groups (aspartate and glutamate), at a slightly increased pH milieu (Zhang et al., 2004). A recent study provided experimental evidence that the hardness of the biosilica within the *M. chuni* GBS is regionally different (Miserez et al., 2008); by focusing on the axial cylinder, Miserez et al. found that the hardness/indentation of the center of the spicules is approximately 2.5 times lower compared with the lamellar region.

In conclusion, the data presented here suggest that a close cell–silica contact is involved in silica formation, as shown here in the sponge *M. chuni*. Prior to this, using both the demosponge (*Suberites domuncula*) and the hexactinellid model (*M. chuni*), no evidence could be presented that filaments, e.g. collagen, are primarily involved in the formation of the silica lamellae (Müller et al., 2009b). Based on the present data, the following steps for the formation of the outer lamella can be formulated (Fig. 1B). Sclerocytes associate to cell clusters on the surface of the (pen)ultimate smooth-surfaced lamella and start to form pericellular silica using silicatein under consumption of silicic acid. After the stage of textured lamella formation, the cell clusters proceed with silica formation and allow the completion of a smooth surface. The cells remain immobilized on the surface of the terminated lamella and attached to the spicule *via* a filamentous network for the next round of lamella formation (Fig. 1C).

REFERENCES

Boury-Esnault, N. and Rützler, K. (1997). Thesaurus of sponge morphology. *Smithson. Contrib. Zool.* **596**, 1-55.

Brunner, E., Richthammer, P., Ehrlich, H., Paasch, S., Simon, P., Ueberlein, S. and van Pee, K.-H. (2009). Chitin-based organic networks – an integral part of cell wall biosilica from the diatom *Thalassiosira pseudonana*. *Angewandte Chemie Intern. Edit.* **48**, 9724-9727.

Butler, P. E. (1961). Morphologic classification of sponge spicules, with descriptions of siliceous spicules from the Lower Ordovician Bellefonte Dolomite in Central Pennsylvania. *J. Paleontol.* **35**, 191-200.

Cha, J. N., Shimizu, K., Zhou, Y., Christianssen, S. C., Chmelka, B. F., Stucky, G. D. and Morse, D. E. (1999). Silicatein filaments and subunits from a marine sponge direct the polymerization of silica and silicones in vitro. *Proc. Natl. Acad. Sci. USA* **96**, 361-365.

Ehrlich, H. (2010). *Biological Materials of Marine Origin. Invertebrates.* Heidelberg: Springer-Verlag.

Ehrlich H. (2011) Silica biomineralization in sponges. In *Encyclopedia of Geobiology* (ed. J. Reitner and V. Thiel), pp. 796-808. Heidelberg: Springer-Verlag.

Ehrlich, H., Heinemann, S., Heinemann, C., Simon, P., Bazhenov, V. V., Shapkin, N. P., Born, R., Tabachnick, K., Hanke, T. and Worch, H. (2008). Nanostructural organization of naturally occurring composites – Part I: silica-collagen-based biocomposites. *J. Nanomat.* **2008**, 623838. doi:10.1155/2008/623838.

Ehrlich, H., Demadis, K. D., Pokrovsky, O. S. and Koutsoukos, P. G. (2010a). Modern views on desilicification: biosilica and abiotic silica dissolution in natural and artificial environments. *Chem. Rev.* **110**, 4656-4689.

Ehrlich, H., Simon, P, Carrillo-Cabrera, W., Bazhenov, V. V., Botting, J., Ilan, M., Ereskovsky, A. V., Muricy, G., Worch, H, Mensch, A. et al. (2010b). Insights into chemistry of biological materials: newly discovered silica-aragonite-chitin biocomposites in demosponges. *Chem. Mat.* **22**, 1462-1471.

Ehrlich, H., Deutzmann, R., Brunner, E., Cappellini, E., Koon, H., Solazzo, C., Yang, Y., Ashford, D., Thomas-Oates, J., Lubeck, M. et al. (2010c). Mineralization of the meter-long biosilica structures of glass sponges is templated on hydroxylated collagen. *Nature Chem.* **2**, 1084-1088

Hildebrand, M. and Wetherbee, R. (2003). Components and control of silicification in diatoms. In *Silicon Biomineralization: Biology, Biochemistry, Molecular Biology, Biotechnology* (ed. W. E. G. Müller), pp. 11-57, Vol. 33. Heidelberg: Springer-Verlag.

Hooper, J. N. A (1997). *Guide to Sponge Collection and Identification.* South Brisbane: Queensland Museum. Available at http://xa.yimg.com/kq/groups/21368769/1183738468/name/Guide+to+sponge+identification.pdf.

Inagaki, F., Motomura, Y. and Ogata, S. (2003). Microbial silica deposition in geothermal hot waters. *Appl. Microbiol. Biotechnol.* **60**, 605-611.

Krasko, A., Batel, R., Schröder, H. C., Müller, I. M. and Müller, W. E. G (2000). Expression of silicatein and collagen genes in the marine sponge *Suberites domuncula* is controlled by silicate and myotrophin. *Eur. J. Biochem.* **267**, 4878-4887.

Kröger, N. and Sumper, M. (2000). The biochemistry of silica formation in diatoms. In *Biomineralization* (ed. E. Bäuerlein), pp. 151-170. Weinheim, New York: Wiley-VCH.

Levi, C., Barton, J. L., Guillemet, C., Lebras, E. and Leheude, P. (1989). A remarkably strong natural glassy rod: the anchoring spicule of the *Monoraphis* sponge. *J. Mat. Sci. Lett.* **8**, 337-339.

Leys, S. P. (2003). Comparative study of spiculogenesis in demosponge and hexactinellid larvae. *Microsc. Res. Tech.* **62**, 300-311.

Leys, S. P., Mackie, G. O. and Reiswig, H. M. (2007). The biology of glass sponges. *Adv. Mar. Biol.* **52**, 1-145.

Li, X. D. and Bhushan B. (2002). A review of nanoindentation continuous stiffness measurement technique and its applications. *Mater. Charact.* **48**, 11-36.

Ma, J. F. (2003). Functions of silicon in higher plants. *Prog. Mol. Subcell. Biol.* **33**, 127-147.

Maldonado, M., Carmona, M. C., Velásquez, Z., Puig, A., Cruzado, A., López, A. and Young, C. M. (2005). Siliceous sponges as a silicon sink: an overlooked aspect of benthopelagic coupling in the marine silicon cycle. *Limnol. Oceanogr.* **50**, 799-809.

Minchin, E. A. (1909). Sponge spicules. A summary of present knowledge. *Ergebn. Forts. Zool.* **2**, 171-274.

Miserez, A., Weaver, J. C., Thurner, P. J., Aizenberg, J., Dauphin, Y., Fratzl, P., Morse, D. E. and Zok, F. W. (2008). Effects of laminate architecture on fracture resistance of sponge biosilica: lessons from nature. *Adv. Funct. Mater.* **18**, 1241-1248.

Morse, D. E. (1999). Silicon biotechnology: harnessing biological silica production to construct new materials. *Trends Biotechnol.* **17**, 230-232.

Mugnaioli, E., Natalio, F., Schloßmacher, U., Wang, X. H., Müller, W. E. G. and Kolb, U. (2009) Crystalline nanorods as seeds for the synthesis of amorphous biosilica during spicule formation in sponges. *Chembiochem* **10**, 683-689.

Müller, W. E. G. (ed.) (2003). *Silicon Biomineralization: Biology, Biochemistry, Molecular Biology, Biotechnology.* Berlin: Springer Press.

Müller, W. E. G., Wiens, M., Adell, T., Gamulin, V., Schröder, H. C. and Müller, I. M. (2004) Bauplan of urmetazoa: basis for genetic complexity of Metazoa. *Intern. Review Cytol.* **235**, 53-92.

Müller, W. E. G., Rothenberger, M., Boreiko, A., Tremel, W., Reiber, A. and Schröder, H. C. (2005). Formation of siliceous spicules in the marine demosponge *Suberites domuncula. Cell Tissue Res.* **321**, 285-297.

Müller, W. E. G., Boreiko, A., Schloßmacher, U., Wang, X. H., Tahir, M. N., Tremel, W., Brandt, D., Kaandorp, J. A. and Schröder, H. C. (2007a). Fractal-related assembly of the axial filament in the demosponge *Suberites domuncula*: relevance to biomineralization and the formation of biogenic silica. *Biomaterials* **28**, 4501-4511.

Müller, W. E. G., Boreiko, A., Wang, X. H., Belikov, S. I., Wiens, M., Grebenjuk, V. A., Schloßmacher, U. and Schröder, H. C. (2007b). Silicateins, the major biosilica forming enzymes present in demosponges: protein analysis and phylogenetic relationship. *Gene* **395**, 62-71.

Müller, W. E. G., Eckert, C., Kropf, K., Wang, X. H., Schloßmacher, U., Seckert, C., Wolf, S. E., Tremel, W. and Schröder, H. C. (2007c). Formation of the giant spicules of the deep sea hexactinellid *Monorhaphis chuni* (Schulze 1904): electron microscopical and biochemical studies. *Cell Tissue Res.* **329**, 363-378.

Müller, W. E. G., Li, J., Schröder, H. C., Qiao, L. and Wang, X. H. (2007d). The unique skeleton of siliceous sponges (Porifera; Hexactinellida and Demospongiae) that evolved first from the Urmetazoa during the Proterozoic: a review. *Biogeosciences* **4**, 219-232.

Müller, W. E. G., Wang, X. H., Belikov, S. I., Tremel, W., Schloßmacher, U., Natoli, A., Brandt, D., Boreiko, A., Tahir, M. N., Müller, I. M. and Schröder, H. C. (2007e). Formation of siliceous spicules in demosponges: example *Suberites domuncula*. In *Handbook of Biomineralization – The Biology of Biominerals Structure Formation* (ed. E. Bäuerlein), Vol. 1, pp. 59-82. Weinheim: Wiley-VCH.

Müller, W. E. G., Engel, S., Wang, X. H., Wolf, S. E., Tremel, W., Thakur, N. L., Krasko, A., Divekar, M. and Schröder, H. C. (2008a). Bioencapsulation of living bacteria (*Escherichia coli*) with poly(silicate) after transformation with silicatein-α gene. *Biomaterials* **29**, 771-779.

Müller, W. E. G., Jochum, K., Stoll, B. and Wang, X. H. (2008b). Formation of giant spicule from quartz glass by the deep sea sponge *Monorhaphis. Chem. Mater.* **20**, 4703-4711.

Müller, W. E. G., Wang, X. H., Kropf, K., Boreiko, A., Schloßmacher, U., Brandt, D., Schröder, H. C. and Wiens, M. (2008c). Silicatein expression in the hexactinellid *Crateromorpha meyeri*: the lead marker gene restricted to siliceous sponges. *Cell Tissue Res.* **333**, 339-351.

Müller, W. E. G., Wang, X. H., Kropf, K., Ushijima, H., Geurtsen, W., Eckert, C., Tahir, M. N., Tremel, W., Boreiko, A., Schloßmacher, U., Li, J. and Schröder, H. C. (2008d). Bioorganic/inorganic hybrid composition of sponge spicules: matrix of the giant spicules and of the comitalia of the deep sea hexactinellid *Monorhaphis. J. Struct. Biol.* **161**, 188-203.

Müller, W. E. G., Schloßmacher, U., Wang, X. H., Boreiko, A., Brandt, D., Wolf, S. E., Tremel, W. and Schröder, H. C. (2008e) Poly(silicate)-metabolizing silicatein in siliceous spicules and silicasomes of demosponges comprises dual enzymatic activities (silica-polymerase and silica-esterase). *FEBS J.* **275**, 362-370.

Müller, W. E. G., Wang, X. H., Burghard, Z., Bill, J., Krasko, A., Boreiko, A., Schloßmacher, U., Schröder, H. C. and Wiens, M. (2009a). Bio-sintering processes in hexactinellid sponges: fusion of bio-silica in giant basal spicules from *Monorhaphis chuni. J. Struct. Biol.* **168**, 548-561.

Müller, W. E. G., Wang, X. H., Cui, F. Z., Jochum, K. P., Tremel, W., Bill, J., Schröder, H. C., Natalio, F., Schloßmacher, U. and Wiens, M. (2009b). Sponge spicules as blueprints for the biofabrication of inorganic-organic composites and biomaterials. *Appl. Microbiol. Biotechnol.* **83**, 397-413.

Neumann, D. (2003). Silicon in plants. In *Silicon Biomineralization: Biology, Biochemistry, Molecular Biology, Biotechnology* (ed. W. E. G. Müller), pp. 149-160, Vol. 33. Berlin: Springer Press.

Panchuk-Voloshina, N., Haugland, R. P., Bishop–Stewart, J., Bhalgat, M. K., Millard, P. J., Mao, F., Leung, W. Y. and Haugland, P. (1999). Alexa dyes, a series of new fluorescent dyes that yield exceptionally bright, photostable conjugates. *J. Histochem. Cytochem.* **47**, 1179-1188.

Perry, C. C. (2003). Silicification: the processes by which organisms capture and mineralize silica. *Rev. Mineral. Geochem.* **54**, 291-327.

Reuter, P., Dorn, A., Batel, R., Schröder, H. C. and Müller, W. E. G. (1987). Evidence for the existence of microtubule protein in the extracellular space of marine sponges. *Tissue Cell* **19**, 773-782.

Sachs, L. (1984). *Angewandte Statistik*. Berlin: Springer.

Schröder, H. C., Perovic-Ottstadt, S., Rothenberger, M., Wiens, M., Schwertner, H., Batel, R., Korzhev, M., Müller, I. M. and Müller, W. E. G. (2004). Silica transport in the demosponge *Suberites domuncula*: fluorescence emission analysis using the PDMPO probe and cloning of a potential transporter. *Biochem. J.* **381**, 665-673.

Schröder, H. C., Boreiko, A., Korzhev, M., Tahir, M. N., Tremel, W., Eckert, C., Ushijima, H., Müller, I. M. and Müller, W. E. G. (2006). Co-expression and functional interaction of silicatein with galectin: matrix-guided formation of siliceous spicules in the marine demosponge *Suberites domuncula. J. Biol. Chem.* **281**, 12001-12009.

Schröder, H. C., Natalio, F., Shukoor, I., Tremel, W., Schloßmacher, U., Wang, X. H. and Müller, W. E. G. (2007). Apposition of silica lamellae during growth of spicules in the demosponge *Suberites domuncula*: biological/biochemical studies and chemical/biomimetical confirmation. *J. Struct. Biol.* **159**, 325-334.

Schröder, H. C., Wiens, M., Schloßmacher, U., Brandt, D. and Müller, W. E. G. (in press). Silicatein-mediated polycondensation of orthosilicic acid: modeling of catalytic mechanism involving ring formation. *Silicon* doi: 10.1007/s12633-010-9057-4.

Schulze, F. E. (1904). *Hexactinellida. Wissenschaftliche Ergebnisse der Deutschen Tiefsee-Expedition auf dem Dampfer "Valdivia"* 1898-1899. Stuttgart: Fischer.

Shimizu, K., Cha, J., Stucky, G.D. and Morse, D.E. (1998). Silicatein alpha: cathepsin L-like protein in sponge biosilica. *Proc. Natl. Acad. Sci. USA* **95**, 6234-6238.

Suzuki, T., Fujikura, K., Higashiyama, T. and Takata, K. (1997). DNA staining for fluorescence and laser confocal microscopy. *J. Histochem. Cytochem.* **45**, 49-53.

Titus, J. A., Haugland, R. P., Sharrow, S. O. and Segal, D. M. (1982). Texas Red, a hydrophilic, red-emitting fluorophore for use with fluorescein in dual parameter flow microfluorometric and fluorescence microscopic studies. *J. Immunol. Methods* **50**, 193-204.

Uriz, M. J. (2006). Mineral spiculogenesis in sponges. *Can. J. Zool.* **84**, 322-356.

Uriz, M.-J., Turon, X., Becero, M. A. and Agell, G. (2003) Siliceous spicules and skeletal frameworks in sponges: origin, diversity, ultrastructural patterns and biological functions. *Microsc. Res. Tech.* **62**, 279-299.

Wang, X. H. and Müller, W. E. G. (2009). Contribution of biomineralization during growth of polymetallic nodules and ferromanganese crusts from the Pacific Ocean. *Front. Mater. Sci. China* **3**, 109-123.

Wang, X. H., Li, J., Qiao, L., Schröder, H. C., Eckert, C., Kropf, K., Wang, Y. M., Feng, Q. L. and Müller, W. E. G. (2007). Structure and characteristics of giant spicules of the deep sea hexactinellid sponges of the genus *Monorhaphis* (Hexactinellida: Amphidiscosida: Monorhaphididae). *Acta Zool. Sin.* **53**, 557-569.

Wang, X. H., Boreiko, A., Schloßmacher, U., Brandt, D., Schröder, H. C., Li, J., Kaandorp, J. A., Götz, H., Duschner, H. and Müller, W. E. G. (2008). Axial growth of hexactinellid spicules: formation of cone-like structural units in the giant basal spicules of the hexactinellid *Monorhaphis. J. Struct. Biol.* **164**, 270-280.

Wang, X. H., Schröder, H. C. and Müller, W. E. G. (2009a). Giant siliceous spicules from the deep-sea glass sponge *Monorhaphis chuni*: morphology, biochemistry, and molecular biology. *Int. Rev. Cell. Mol. Biol.* **273**, 69-115.

Wang, X. H., Schloßmacher, U., Wiens, M., Schröder, H. C. and Müller, W. E. G. (2009b) Biogenic origin of polymetallic nodules from the Clarion-Clipperton zone in the Eastern Pacific Ocean: electron microscopic and EDX evidence. *Mar. Biotechnol.* **11**, 99-108.

Weissenfels, N. (1989). *Biologie und Mikroskopische Anatomie der Süßwasserschwämme (Spongillidae)*. Stuttgart, New York: Gustav Fischer Verlag.

Wiederhorn, S. M. (1969). Fracture stress energy of glass. *J. Am. Ceram. Soc.* **52**, 99-105.

Wiens, M., Bausen, M., Natalio, F., Link, T., Schlossmacher, U. and Müller, W. E. G. (2009). The role of the silicatein-a interactor silintaphin-1 in biomimetic biomineralization. *Biomaterials* **30**, 1648-1656.

Wiens, M., Wang, X. H., Schloßmacher, U., Lieberwirth, I., Glasser, G., Ushijima, H., Schröder, H. C. and Müller, W. E. G. (2010). Osteogenic potential of bio-silica on human osteoblast-like (SaOS-2) cells. *Calcif. Tissue Int.* **87**, 513-524.

Wiens, M., Schröder, H. C., Wang, X. H., Link, T., Steindorf, D. and Müller, W. E. G. (2011). Isolation of the silicatein-α interactor silintaphin-2 by a novel solid-phase pull-down assay. *Biochemistry* **50**, 1981-1990.

Zhang, L. J., Feng, X. S., Liu, H. G., Qian, D. J., Zhang, L., Yu, X. L. and Cui, F. Z. (2004). Hydroxyapatite/collagen composite materials formation in simulated body fluid environment. *Materials Lett.* **58**, 719-722.